

Article

# A Novel Magnetic Flux Leakage Method Incorporating TMR Sensors for Detecting Zinc Dross Defects on the Surface of Hot-Dip Galvanized Sheets

Bo Wang<sup>1,\*</sup>, San Zhang<sup>2</sup>, Jie Wang<sup>3</sup>, Liqin Jing<sup>1</sup> and Feilong Mao<sup>1</sup><sup>1</sup> Department of Mechanical and Electrical, Yuncheng University, Yuncheng 044000, China<sup>2</sup> School of Automation, Xi'an University of Posts & Telecommunications, Xi'an 710121, China<sup>3</sup> Metallurgical Technology Institute, Central Iron and Steel Research Institute, Beijing 100081, China

\* Correspondence: wangbo199027@126.com

**Abstract:** Surface quality control of hot-dip galvanized sheets is a critical research topic in the metallurgical industry. Zinc dross, the most common surface defect in the hot-dip galvanizing process, significantly affects the sheet's service performance. In this manuscript, a novel magnetic flux leakage (MFL) detection method was proposed to detect zinc dross defects on the surface of hot-dip galvanized steel sheets. Instead of using exciting coils in traditional methods, a tiny permanent magnet with a millimeter magnitude was employed to reduce the size and weight of the equipment. Additionally, a high-precision tunnel magnetoresistance (TMR) sensor with a sensitivity of 300 mV/V/Oe was selected to achieve higher detection accuracy. The experimental setup was established, and the x-axis direction (sample movement direction) was determined as the best measurement axis by vector analysis through experiments and numerical simulation. The detection results indicate that this novel MFL detection method could detect industrial zinc dross with an equivalent size of 400  $\mu\text{m}$ , with high signal repeatability and signal-to-noise ratio. In the range of 0–1200 mm/s, the detection speed has almost no effect on the measurement signal, which indicates that this novel method has higher adaptability to various conditions. The multi-path scanning method with a single probe was used to simulate the array measurement to detect a rectangular area of 30  $\times$  60 mm. Ten zinc dross defects were detected across eight measurement paths with 4 mm intervals, and the positions of these zinc dross defects were successfully reconstructed. The research results indicate that this novel MFL detection method is simple and feasible. Furthermore, the implementation of array measurements provides valuable guidance for subsequent in-depth research and potential industrial applications in the future.

**Keywords:** magnetic flux leakage; hot-dip galvanized sheet; zinc dross; array measurement; tunnel magnetoresistance sensor



**Citation:** Wang, B.; Zhang, S.; Wang, J.; Jing, L.; Mao, F. A Novel Magnetic Flux Leakage Method Incorporating TMR Sensors for Detecting Zinc Dross Defects on the Surface of Hot-Dip Galvanized Sheets. *Magnetochemistry* **2024**, *10*, 101. <https://doi.org/10.3390/magnetochemistry10120101>

Academic Editor: Evangelos Hristoforou

Received: 9 November 2024

Revised: 7 December 2024

Accepted: 9 December 2024

Published: 10 December 2024



**Copyright:** © 2024 by the authors. Licensee MDPI, Basel, Switzerland. This article is an open access article distributed under the terms and conditions of the Creative Commons Attribution (CC BY) license (<https://creativecommons.org/licenses/by/4.0/>).

## 1. Introduction

In steel materials, hot-dip galvanized sheets [1–3] have been widely used in sectors such as lightweight automotive, light industry, home appliances, and agriculture [4] due to their high strength, corrosion resistance, and formability. These sheets play an increasingly important role in modern economic and social development, permeating many aspects of daily life. With advancements in steel industry technology, downstream industries like home appliances and automotive manufacturing have become more stringent in their requirements for the surface quality of hot-dip galvanized sheets. The level of inclusions on the surface of these sheets greatly impacts their performance in engineering applications.

During the production process of hot-dip galvanized sheets, zinc dross defects [5–7] are difficult to avoid in the coating layer. It is a non-ferromagnetic Zn–Fe compound and appears as irregular granular inclusions or blocks on the surface of the sheet. The primary sources of zinc dross include the carryover of zinc ash from furnace residue, accumulation

of bottom and suspended dross, and surface dross adhesion. Additionally, factors such as fluctuations in zinc pot temperature, incomplete dross removal, overuse of the submerged roll, and excessive aluminum content may contribute to the formation of zinc dross. Most zinc dross is brought during the galvanizing process and becomes flattened under rolling pressure, significantly affecting surface quality. Detecting and controlling zinc dross defects during the galvanizing process have become valuable research topics in the metallurgical industry. At present, the detection of zinc dross defects on galvanized sheet surfaces primarily relies on visual inspection, which has gone through three major stages: manual visual inspection, traditional photoelectric detection, and machine vision [8]. Manual visual inspection identifies defects by eye, but it suffers from low sampling rates, limited accuracy, poor real-time performance, low efficiency, and high labor intensity, making it feasible only in a few scenarios. The development of machine vision inspection has been driven by advancements in image processing and analysis algorithms. However, each algorithm has its own advantages/disadvantages and application conditions despite continuous updates. Improving algorithm efficiency, accuracy, real-time performance, and adaptability remains a key area for advancement.

Magnetic flux leakage (MFL) detection [9–17] is a traditional non-destructive testing method primarily used in detecting defects in ferromagnetic materials like oil pipelines, where it is commonly known as the “pipeline pig” [10–12]. This method typically involves sensors detecting the leakage field caused by surface defects that interrupt the material’s continuity, thereby identifying defect size and location. Recently, MFL detection has been widely adopted for its non-contact nature, high sensitivity, and low cost, as well as its ability to detect small defects [12]. Traditional MFL methods often use coil-type excitation magnets, which provide adjustable magnetic fields but tend to be large and heavy. Magnetic sensors, usually Hall elements or induction coils, have limited detection accuracy.

In this study, an improved MFL detection method was proposed based on the traditional method. A small permanent magnet with a millimeter scale was employed to replace the coil excitation used in traditional methods, significantly reducing the device’s size and weight. High-precision tunnel magnetoresistance (TMR) sensors with a sensitivity of 300 mV/V/Oe were used to enhance detection accuracy. This novel MFL detection method was applied to detecting zinc dross defects on hot-dip galvanized sheet surfaces, with a focus on detection performance and defect location reconstruction, aiming to provide technical support for further improvements in the surface quality of galvanized sheets.

## 2. Novel Magnetic Flux Leakage Detection Method

### 2.1. Basic Principle

The basic principle of the novel MFL detection method is illustrated in Figure 1. The ferromagnetic specimen is magnetized by an adjacent permanent magnet. If the specimen has no defects, the magnetic flux generated by the external magnetic field remains confined within the specimen, with smooth and undisturbed flux lines. However, if the specimen contains defects, the magnetic permeability in the defect area is much lower than that of the ferromagnetic specimen, which causes a sharp increase in magnetic resistance at the defect area. As a result, the magnetic flux lines in the defect area become distorted, the magnetic field direction changes, and magnetic poles form, creating a leakage magnetic field over the defect region. Numerical simulations in Figure 2 also verify this principle. By using a magnetic-sensitive sensor to detect the MFL field, the corresponding signal can be obtained, and analyzing this signal reveals information about the defect.

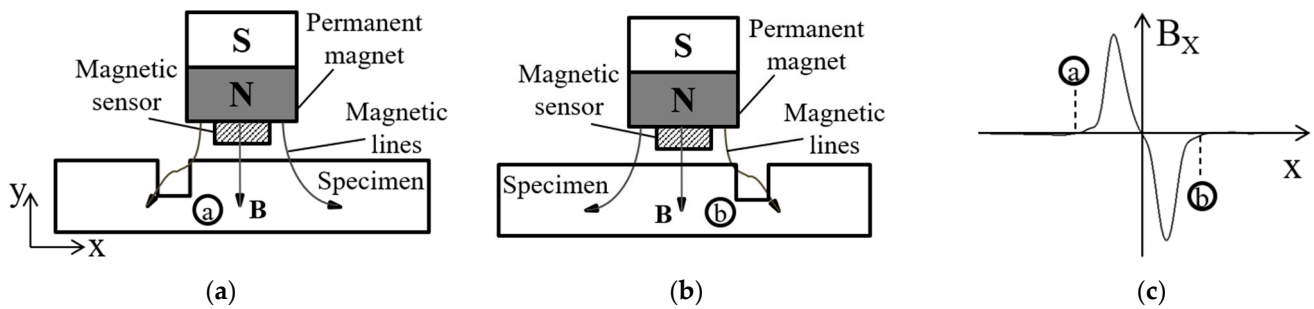


**Figure 1.** Principle sketch of the novel MFL method: (a) defect near, (b) leave the permanent magnet, and (c) characteristic of the signal.

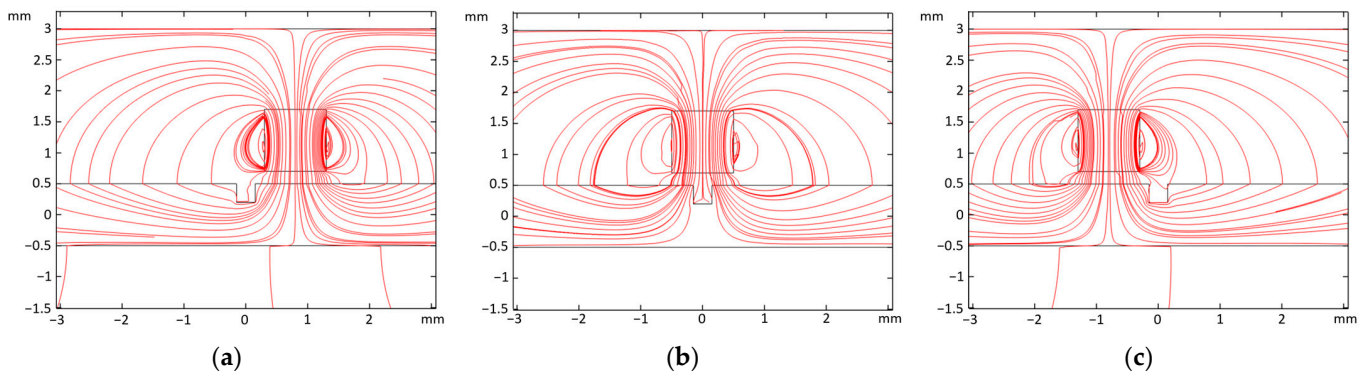


**Figure 2.** Evolution of magnetic lines when a ferromagnetic material with defect passes through a permanent magnet: (a) defect near, (b) underneath, and (c) leave the PM.

## 2.2. Tunnel Magnetoresistance (TMR) Sensor

Magnetic sensors are widely used in modern industry and electronic products. In order of emergence, a magnetic sensor mainly includes the differential coil [18], hall sensor [19], anisotropic magnetoresistance (AMR) [20], giant magnetoresistance (GMR) [21], magneto optical (MO) sensors [22], and tunnel magnetoresistance (TMR) sensors [23]. Each sensor has its own advantages and disadvantages. For example, Hall sensors achieve high output sensitivity by using flux concentrator structures to amplify the magnetic field, which increases the sensor's size and weight. Hall sensors also suffer from high power consumption and poor linearity. AMR sensors have improved sensitivity than Hall sensors but have a narrower linear range. Additionally, AMR sensors require preset/reset coils, which add complexity, size, and power consumption. GMR sensors have higher sensitivity than Hall sensors but have limited linear ranges.

Developed based on the tunnel magnetoresistance effect [24], TMR sensors are more sensitive and have recently begun to be used in industrial applications. TMR sensors have a higher rate of resistance change than AMR and GMR sensors. Compared to Hall, AMR, and GMR sensors, TMR sensors exhibit better temperature stability, linearity, higher sensitivity, lower power consumption, a wider linear range, and do not require AMR's additional preset/reset coils. It is reported [23] that TMR sensors surpass traditional magnetic sensors in sensitivity and linear operating range. Table 1 summarizes a comparison of typical technical parameters of various magnetic sensors, clearly showing the advantages of TMR sensors.

The high-precision TMR sensor (model TMR9001, provided by Multidimensional Technology Co., Ltd, Suzhou, China.) used in this study features a unique push-pull Wheatstone full-bridge structure with four highly sensitive TMR elements. It is packaged in SOP8 format (6 mm × 5 mm × 1.5 mm). The TMR9001 sensor is single-axis sensitive, with sensitivity up to 300 mV/V/Oe and typical background noise as low as 150 pT/√(Hz) at 1 Hz. Additionally, the TMR9001 offers ultra-low power consumption, excellent temperature stability, very low hysteresis, and a wide operating voltage range.

It also eliminates the need for preset or reset pulse circuits, simplifying the measurement process and enhancing reliability.

**Table 1.** Comparison of technical parameters for various magnetic sensors [25].

| Technology | Power Consumption (mA) | Size (mm) | Sensitivity (mV/V/Oe) | Operating Range (Oe) | Resolution (mOe) | Temperature Characteristics (°C) |
|------------|------------------------|-----------|-----------------------|----------------------|------------------|----------------------------------|
| Hall       | 5~20                   | 1 × 1     | 0.05                  | 1~1000               | 500              | <150                             |
| AMR        | 1~10                   | 1 × 1     | 1                     | 0.001~10             | 0.1              | <150                             |
| GMR        | 1~10                   | 2 × 2     | 3                     | 0.1~30               | 2                | <150                             |
| TMR        | 0.001~0.01             | 0.5 × 0.5 | 20                    | 0.001~200            | 0.1              | <200                             |

### 3. Detection of Zinc Dross in Hot-Dip Galvanized Sheets

#### 3.1. Hot-Dip Galvanized Sheet Specimens

A hot-dip galvanized sheet specimen provided by a steel company is shown in Figure 3, with the black circles indicating visible clusters of point-like inclusions. The thickness of this model of hot-dip galvanized sheet is 0.8 mm, with a carbon steel layer serving as a ferromagnetic material, while the 7 µm thick high-purity zinc coating is conductive but non-ferromagnetic. Irregularly shaped point-like zinc dross inclusions are present in the coating, as indicated by the black circles in Figure 3.

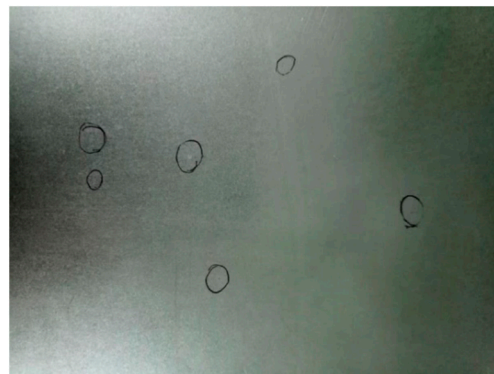


**Figure 3.** Hot-dip galvanized sheet specimen.

In this study, three zinc dross defects marked in Figure 3 were selected as measurement targets, numbered defects 1, 2, and 3. Electron microscope images of three defects are shown in Figure 4. It can be observed that the zinc dross in the coating is clustered in an irregular pattern. By comparing with standard sizes, the equivalent sizes of the inclusions in the three specimens are approximately 396 µm, 405 µm, and 385 µm, respectively.

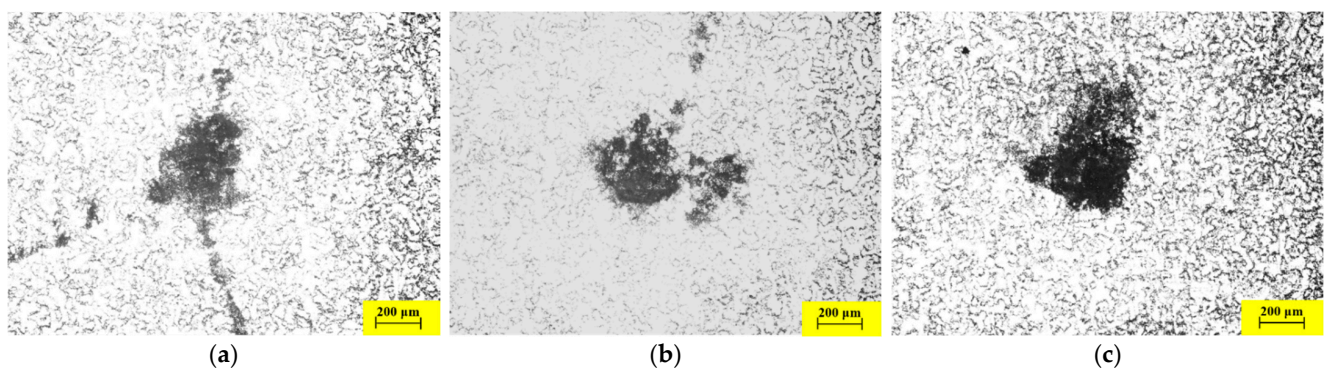


**Figure 4.** Micrographs of zinc dross defects in hot-dip galvanized sheet specimen: (a) defect 1; (b) defect 2; and (c) defect 3.

### 3.2. Experimental Setup

#### 3.2.1. Measurement Device

The measurement device used in this study is shown in Figure 5. It uses a 2 mm cubic permanent magnet as the excitation field, and the high-precision TMR sensor described in Section 2.2 is positioned directly under the permanent magnet. The testing process is as follows: first, the specimen is fixed on a translation stage, and a level gauge is used to adjust the stage to ensure that the specimen is acclinic, reducing the influence of surface irregularity of the specimen on measurement. Next, the sensor is placed directly above the specimen, and the distance between the sensor and the specimen's surface is set to 0.3 mm. The translation stage is then controlled to move at a constant speed of 4.8 mm/s. Finally, the marked inclusion area passes through the magnetic-sensitive area of the permanent magnet, and the measurement signal is captured and recorded using a digital oscilloscope (MDO3022, Tektronix, Shanghai, China).

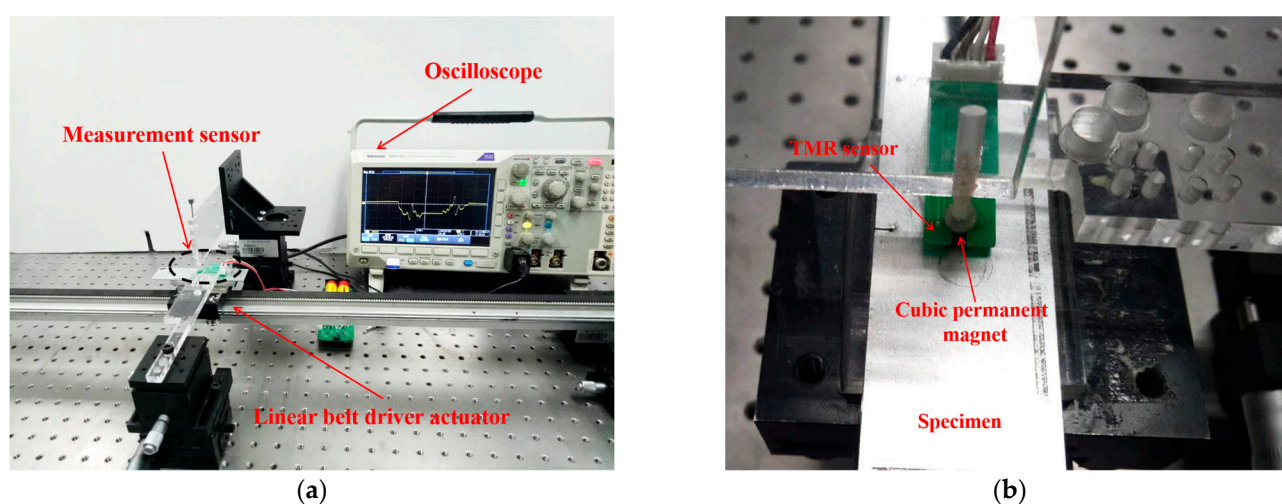


**Figure 5.** Experimental device: (a) overall layout and (b) device details.

#### 3.2.2. Selection of Measurement Axis

Due to the vector characteristics of the leakage magnetic field, vector analysis was conducted on the detection of zinc dross in hot-dip galvanized sheets using both experimental measurements and numerical simulation to achieve better detection results. The numerical model is shown in Figure 6, with parameters matching those of the experiment. The origin of the coordinate system is located at the geometric center of the rectangular ferromagnetic steel sheet, and the specimen moves in the x-axis direction. The steel sheet has a relative magnetic permeability  $\mu_r = 4000$ , relative permittivity  $C = 1$ , and conductivity  $\sigma = 1.12 \times 10^7$  S/m. In the experimental measurements, Specimen 1 from Figure 4 was used as the object of measurement and analysis. Since the TMR9001 sensor is single-axis sensitive, the sensor was rotated  $90^\circ$  to measure the MFL signals in three directions. Experimental and simulated vector measurement results are shown in Figure 7.

In the experimental results in Figure 7a, MFL signals were detected in all three axis directions. The signals in the x and y directions resemble sinusoidal waves, while the z-axis signal shows a negative pulse shape. The signal amplitudes in the x and z directions are similar, both at least an order of magnitude larger than in the y direction. The numerical simulation results in Figure 7b match the experimental signal characteristics and amplitudes, confirming the reliability of the experimental measurements. The numerical model assumes ideal symmetry, so the changes of physical quantities in the y-axis (perpendicular to the motion direction) are theoretically symmetrical and cancel out, producing no MFL signal. However, slight asymmetries in the model's mesh division cause minor variations on either side of the defect, resulting in a small y-axis signal, as shown in Figure 7b. The presence of a y-axis MFL signal in the experimental measurements is attributed to the

irregular morphology of the zinc cross, which breaks the symmetry in the y-axis. Based on the experimental and numerical simulation results in Figure 7, the leakage magnetic field in the x-axis (specimen movement direction) is selected as the measurement target in the present study, with subsequent measurement signals representing the Bx component of the leakage magnetic field.

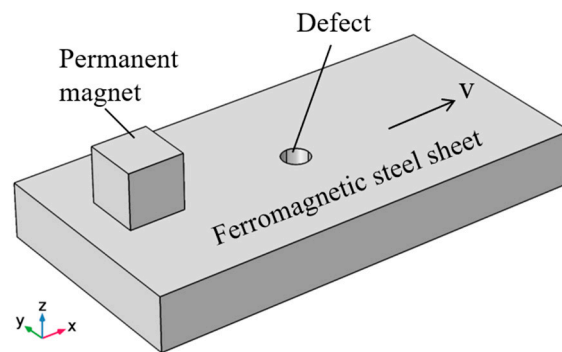


**Figure 6.** Numerical model of vector analysis of galvanized sheet.

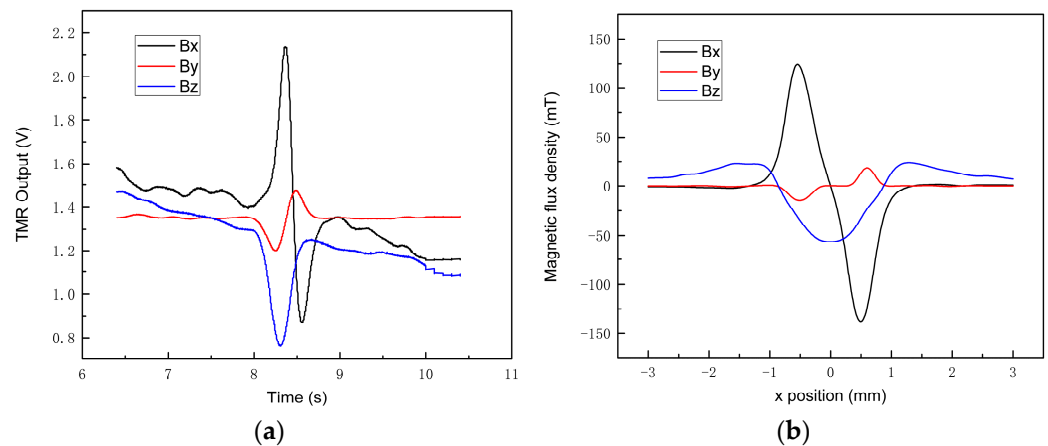


**Figure 7.** The vector analysis results of (a) experimental and (b) numerical study.

### 3.3. Measurement Results and Analysis

The measurement results for the three zinc cross defect measurement points are shown in Figure 8. Each measurement point was measured in two opposite translation directions. From Figure 8, it is clear that the measurement signal caused by the inclusion particles is very distinct, showing an approximately sinusoidal pulse characteristic, consistent with the TMR magnetoresistance sensor's signal characteristics. The signals in opposite directions are mirror images, exhibiting near-symmetrical distribution, indicating good repeatability. This suggests that the novel MFL detection method proposed in this study can be applied to detect inclusions and defects in ferromagnetic materials, such as hot-dip galvanized sheets. It is worth noting that there are certain fluctuations in the baseline background before and after the signal caused by the inclusion particles. This is due to the specimen's surface unevenness. TMR sensor is highly sensitive to the surface flatness of the specimen. Therefore, future studies and industrial applications should aim to reduce interference from surface irregularities in order to minimize background noise signals.

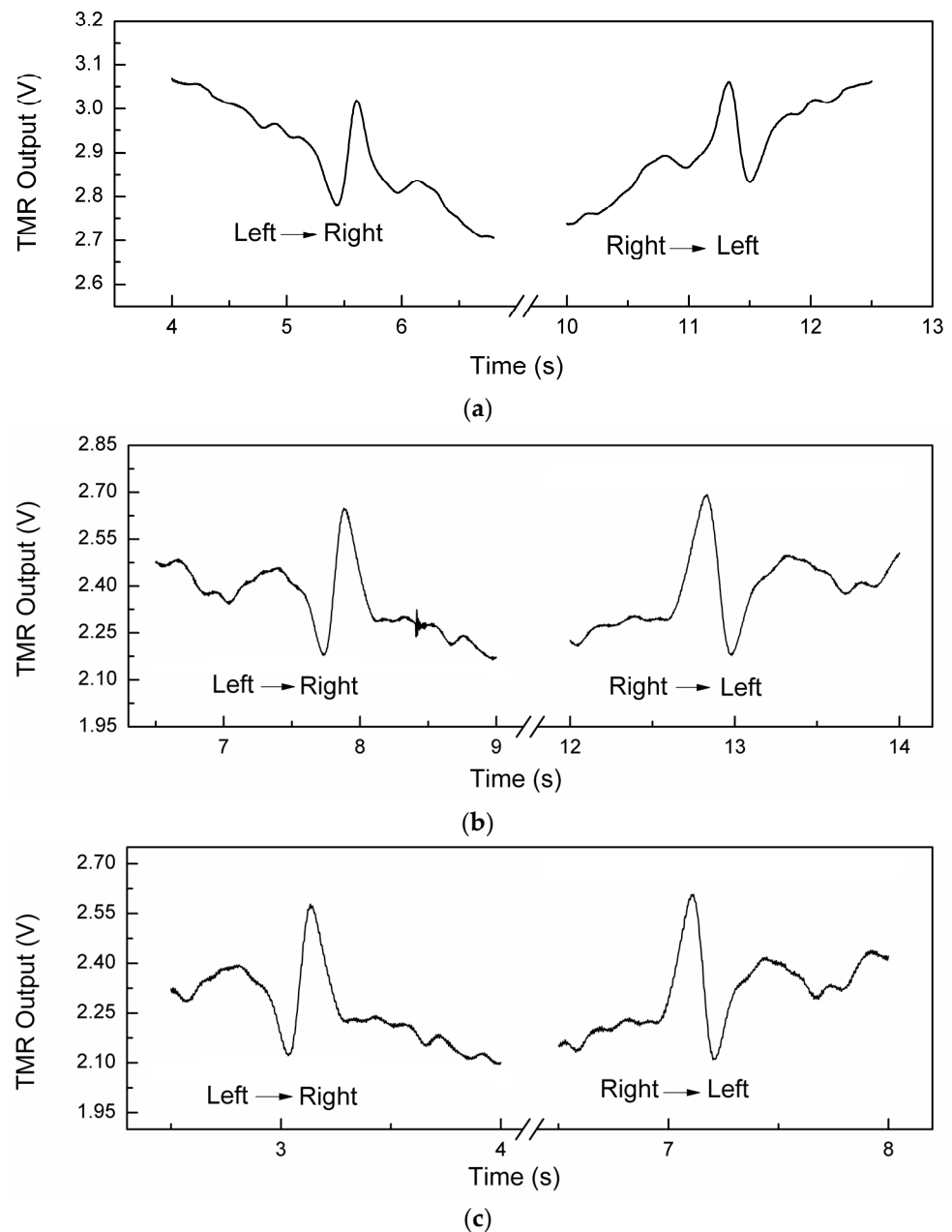


**Figure 8.** Measuring results of galvanized sheet specimen: (a) defect 1; (b) defect 2; and (c) defect 3.

In traditional MFL methods, the speed of the detection device or specimen can impact the measurement results [26]. This study also explored the effect of specimen detection speed on the detection signal. The amplitude of the magnetic leakage signal  $\Delta V$  was selected to indicate signal variation. The results are shown in Figure 9. It is evident that within a speed range of 0–1200 mm/s, detection speed has no significant impact on the detection signal; the signal amplitude  $\Delta V$  remains nearly consistent at different speeds. This is because, under the low-speed conditions in this study, the magnetic Reynolds number [27]  $R_m = \mu_0 \sigma u L \ll 1$ , meaning that the secondary magnetic field generated by induction is negligible, and the magnetic leakage field primarily originates from the magnetization field induced by the permanent magnet. This result suggests that the novel MFL detection method is nearly unaffected by detection speed in industrial applications, allowing it to better adapt to various working conditions.

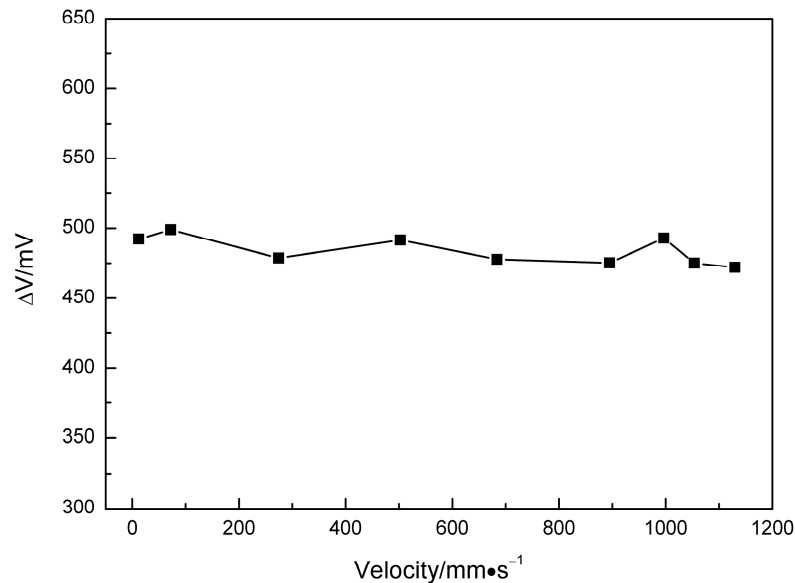


**Figure 9.** Relationship between the moving velocity of the galvanized sheet and the amplitudes of the measuring signals.

### 3.4. Exploration of Array Measurement

In modern industrial technology, measurements are often no longer focused on a single path or small area. As industrial production capabilities expand, larger areas need to be measured, and single-sensor applications are increasingly limited. With the rapid development of measurement technology, array sensors have emerged to handle rapid, large-area measurement tasks, especially in industries requiring online, in-situ, real-time measurement. This study also conducted an initial exploration of array measurement. As shown in Figure 10, the approach of scanning the specimen with a single probe in an S-shaped path to simulate array measurement was involved. The red arrows indicate the direction of each scan path. The scanning area is a rectangular region of  $30 \times 60$  mm. A total of eight scan paths with 4 mm intervals are produced. The first and eighth paths are 1 mm from the edges of the scan area, and the sensor's movement speed is 4.8 mm/s.

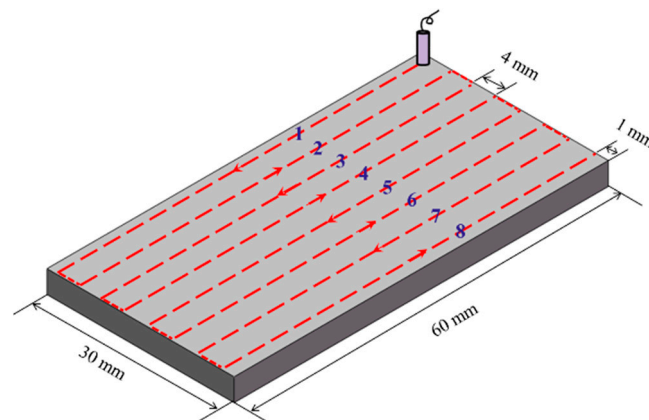


**Figure 10.** Schematic diagram of area scanning paths using a single sensor.

Using the scanning method illustrated in Figure 10, the measurement signals within the scan area were obtained, as shown in Figure 11. Measurement signals from each pair of adjacent paths are plotted together, with detected signal features numbered sequentially in the order of appearance. On path 1, two distinct inclusion signals appear, and the signal amplitude of defect ① was significantly smaller than ②. No significant signal features appear on path 2. Path 3 shows a signal feature at the end of the scan, and path 4 displays two signal features with different amplitudes in the middle region. Path 5 lacks significant

signal features, path 6 shows a distinct signal feature in the central region, path 7 exhibits a prominent signal feature at the start of the scan, and path 8 shows three distinct signals with decreasing amplitudes. Baseline fluctuations on all eight paths are due to the specimen's surface unevenness.

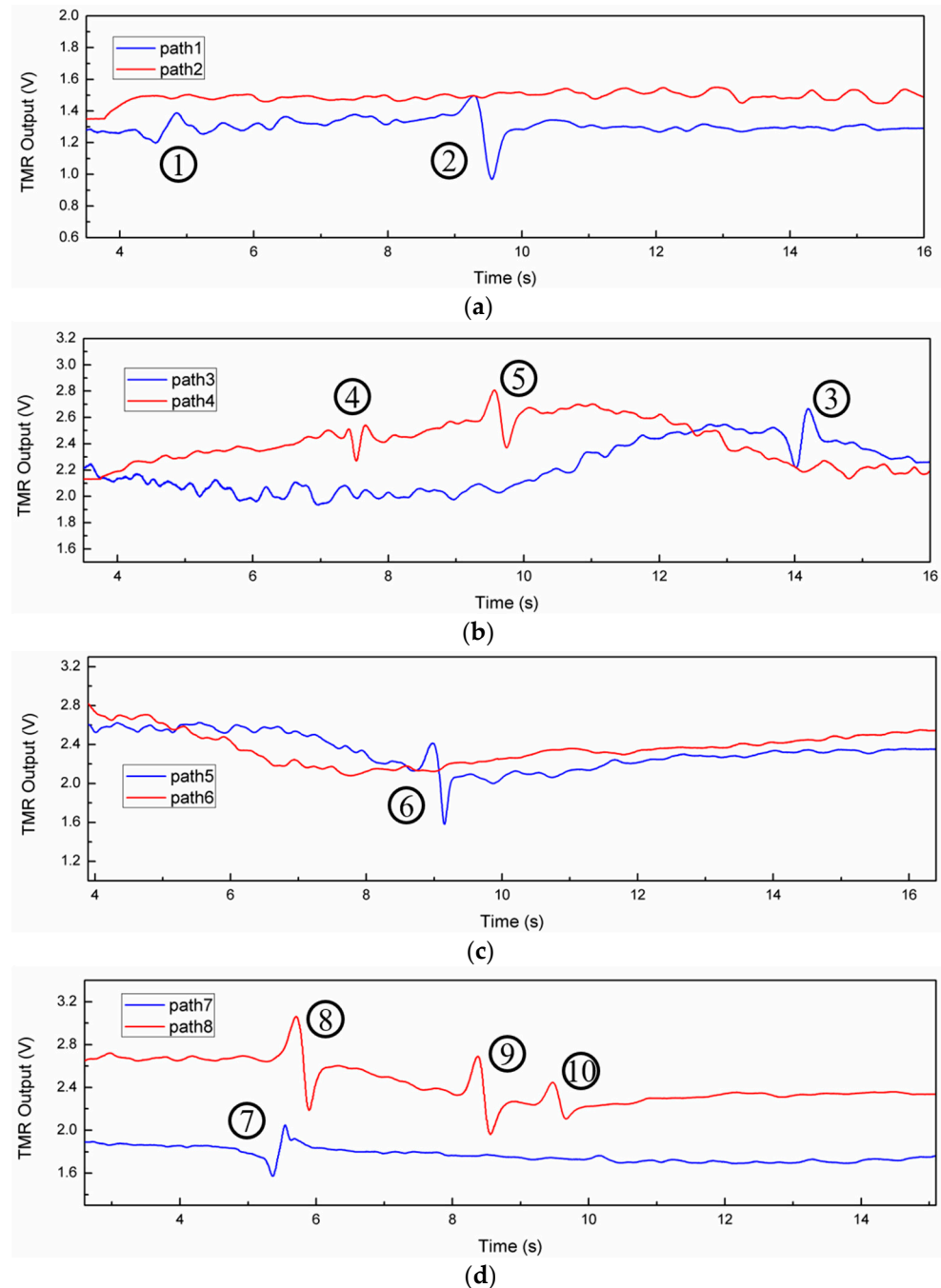


**Figure 11.** Area scanning results using a single sensor: (a) path 1 and 2; (b) path 3 and 4; (c) path 5 and 6; (d) path 7 and 8.

Through the analysis of each of the eight scan paths with a single probe, a total of 10 zinc cross defects were detected in the  $30 \times 60$  mm rectangular measurement area. Based on the detection speed and the time at which the characteristic signals appeared, the exact positions of the zinc cross defects along each path can be calculated, thereby completing the position inversion of the zinc cross defects, as shown in Figure 12. Therefore, the use of array sensors allows for precise localization of inclusion defects, playing a

crucial role in monitoring inclusions in industrial production. In future work, by further controlling experimental conditions and establishing a quantitative relationship between the measurement signal and the size of inclusion defects, it will be possible to obtain size information for the defects, which is highly beneficial for industrial practice.

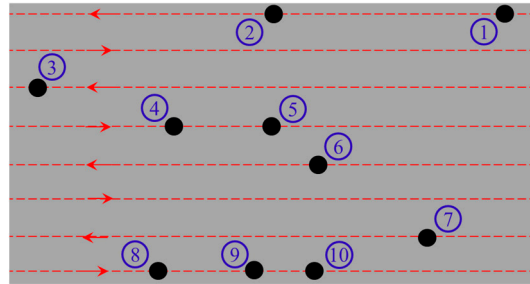


**Figure 12.** Reappearance of zinc dross in a galvanized sheet.

In industrial practice, although scanning back and forth with a single probe can achieve array-type surface scanning, it is time-consuming and inefficient and unable to meet the requirements for online, in-situ, real-time monitoring in thin plate production lines. A feasible solution is to implement multi-sensor array measurements, as shown in Figure 13. The spacing between adjacent sensors should be set to avoid overlap or interference in the excitation magnetic fields. Additionally, to prevent missed detections caused by large gaps between sensors, two or even multiple rows of measurement sensors can be arranged in a staggered configuration. Placing this arrangement on a hot-dip galvanized sheet production line can achieve online, in-situ, real-time monitoring of zinc dross defects without interfering with the production process. This will be a key direction in future research.

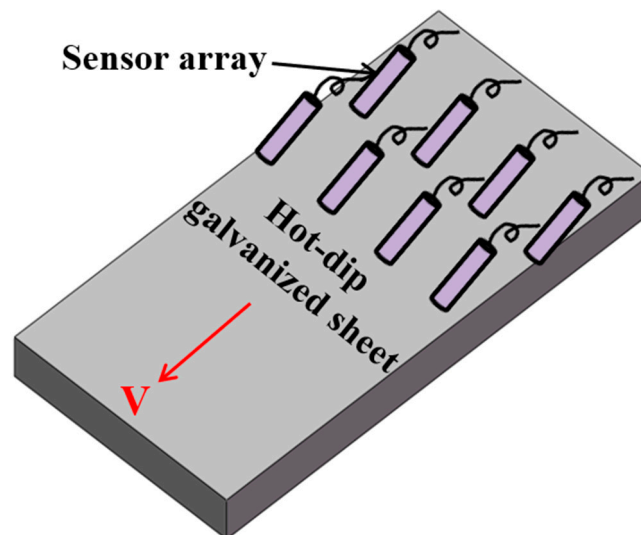


**Figure 13.** Schematic diagram of scanning a galvanized sheet by staggered multi-row array sensors.

#### 4. Conclusions

In this manuscript, a novel MFL detection method is proposed to detect the zinc dross defects on the surface of a hot-dip galvanized sheet. A tiny permanent magnet with a millimeter size as a replacement for the coil excitation used in traditional methods. A high-precision tunnel magnetoresistance (TMR) sensor with a sensitivity of 300 mV/V/Oe was selected, enabling high detection accuracy with a compact and lightweight measurement device. The experimental setup was developed, and the x-axis direction (specimen movement direction) was selected as the optimal measurement axis using experimental and

numerical analysis. A series of measurements, including single and multi-path scanning, were conducted to verify the reliability of the measurement method.

In summary, the MFL detection method proposed in this work could quickly and accurately measure the zinc slag defects on the surface of hot-dip galvanized steel sheets. Compared to traditional methods, it significantly reduces the size and weight of the detection device while markedly improving detection accuracy. Research results indicate that this novel MFL detection method is simple and feasible. It is hoped that the research will provide robust technical support for improving the surface quality and service performance of hot-dip galvanized steel sheets. Futural research will focus on the potential industrial application.

**Author Contributions:** Conceptualization, methodology, formal analysis, investigation, writing—original draft, B.W.; writing—review and editing, data curation, validation, visualization, B.W., S.Z. and L.J.; supervision, resources, J.W.; project administration, funding acquisition, B.W. and F.M. All authors have read and agreed to the published version of the manuscript.

**Funding:** This research was funded by the Fundamental Research Program of Shanxi Province [Grant Number 202303021212265]; the Scientific and Technological Innovation Programs of Higher Education Institutions in Shanxi [Grant Number 2022L487]; the Doctoral Research Launch Project of Yuncheng University [Grant Number YQ-2022004 and YQ-2019005].

**Data Availability Statement:** Data are available from the authors upon reasonable request.

**Conflicts of Interest:** The authors declare no conflicts of interest.

## References

1. Katsuya, H.; Masayasu, N.; Wataru, T.; Yuji, Y.; Shinichi, F.; Matsuzak, A.; Naoto, Y. Effect of Al-based oxide layer on frictional properties of hot-dip galvanized steel sheets. *ISIJ Int.* **2017**, *57*, 895–904.
2. Tokuda, K.; Goto, Y.; Saito, M.; Takebayashi, H.; Konishi, T.; Fukuda, Y.; Nakamura, F.; Kawanishi, K.; Ueda, K.; Shindo, H. New corrosion-resistant Zn-Al-Mg alloy hot-dip galvanized steel sheet. *Corros. Sci. Technol.* **2024**, *23*, 121–130.
3. Kim, D.; Takata, N.; Yokoi, H.; Suzuki, A.; Kobashi, M. Microstructural factors controlling crack resistance of Zn–Al–Mg alloy coatings prepared via hot-dip galvanizing process: Combined approach of in-situ SEM observation with digital image correlation analysis. *J. Mater. Res. Technol.* **2024**, *29*, 1535–1541. [[CrossRef](#)]
4. Ha, H.Y.; Park, S.J.; Kang, J.Y.; Kim, H.D.; Moon, M.B. Interpretation of the corrosion process of a galvanized coating layer on dual-phase steel. *Corros. Sci.* **2011**, *53*, 2430–2436. [[CrossRef](#)]
5. Luo, Q.; Jin, F.; Li, Q.; Zhang, J.Y.; Chou, K.C. The Mechanism of Dross Formation during Hot-dip Al-Zn Alloy Coating Process. *J. Manuf. Sci. Prod.* **2013**, *13*, 85–89. [[CrossRef](#)]
6. Xu, J.; Gu, Q.F.; Li, Q.; Lu, H.S. Influence of Ti and La Additions on the Formation of Intermetallic Compounds in the Al-Zn-Si Bath. *Met. Mater. Trans. A* **2016**, *47*, 6542–6554. [[CrossRef](#)]
7. Luo, X.W.; Lu, H.B.; Zhong, Y.B.; Ren, W.L.; Lei, Z.S. Study of flow and zinc dross removal in hot-dip galvanizing with combined traveling magnetic field. *Materials* **2024**, *17*, 4799. [[CrossRef](#)]
8. Zhao, Z.Q.; Zheng, P.; Xu, S.T.; Wu, X. Object detection with deep learning: A review. *IEEE Trans. Neural Netw. Learn. Syst.* **2019**, *30*, 3212–3232. [[CrossRef](#)]
9. Fang, Z.H.; Zhao, M.; Qian, H.H.; Ding, N.; Li, N. Defect width estimation of magnetic flux leakage signal with wavelet scattering transform. *J. Nondestruct. Eval.* **2024**, *43*, 46. [[CrossRef](#)]
10. Shi, Y.; Zhang, C.; Li, R.; Cai, M.; Jia, G. Theory and application of magnetic flux leakage pipeline detection. *Sensors* **2015**, *15*, 31036–31055. [[CrossRef](#)]
11. Wagner, R.; Goncalves, O.; Demma, A.; Lowe, M. Guided wave testing performance studies: Comparison with ultrasonic and magnetic flux leakage pigs. *Insight-Non-Destr. Test. Cond. Monit.* **2013**, *55*, 187–196. [[CrossRef](#)]
12. Feng, B.; Wu, J.; Tu, H.; Tang, J.; Kang, Y. A review of magnetic flux leakage nondestructive testing. *Materials* **2022**, *15*, 7362. [[CrossRef](#)] [[PubMed](#)]
13. Trevino, D.A.G.; Dutta, S.M.; Ghorbel, F.H.; Karkoub, M. An improved dipole model of 3-D magnetic flux leakage. *IEEE Trans. Magn.* **2016**, *52*, 6201707. [[CrossRef](#)]
14. Han, W.; Xu, J.; Zhou, M.; Tian, G.; Wang, P.; Shen, X.; Hou, E. Cuckoo search and particle filter-based inverting approach to estimating defects via magnetic flux leakage signals. *IEEE Trans. Magn.* **2016**, *52*, 6200511. [[CrossRef](#)]
15. Qiu, J.L.; Zhang, W.P.; Jing, Y. Quantitative linear correlation between self-magnetic flux leakage field variation and corrosion unevenness of corroded rebars. *Measurement* **2023**, *218*, 113173. [[CrossRef](#)]
16. Zhang, S.X.; Feng, J.; Lu, S.X.; Dong, X.; Yao, Y. Weak magnetic flux leakage detection and numerical method under inclined pressure conditions. *IEEE Trans. Magn.* **2023**, *59*, 4600409. [[CrossRef](#)]

17. Ege, Y.; Coramik, M. A new measurement system using magnetic flux leakage method in pipeline inspection. *Measurement* **2018**, *123*, 163–174. [[CrossRef](#)]
18. Yang, L.J.; Liu, G.; Zhang, G.G.; Gao, S.W. Sensor development and application on the oil-gas pipeline magnetic flux leakage detection. In Proceedings of the Ninth International Conference on Electronic Measurement & Instruments, Beijing, China, 16–19 August 2009.
19. Shiogai, J.; Jin, Z.; Satake, Y.; Fujiwara, K.; Tsukazaki, A. Low-frequency noise measurements on Fe–Sn Hall sensors. *Appl. Phys. Express* **2019**, *12*, 123001. [[CrossRef](#)]
20. Wang, C.; Su, W.; Hu, Z.; Pu, J.; Guan, M.; Peng, B.; Li, L.; Ren, W.; Zhou, Z.; Jiang, Z.; et al. Highly sensitive magnetic sensor based on anisotropic magnetoresistance effect. *IEEE Trans. Magn.* **2018**, *54*, 2301103. [[CrossRef](#)]
21. Tehranchi, M.M.; Ranjbaran, M.; Eftekhari, H. Double core giant magneto-impedance sensors for the inspection of magnetic flux leakage from metal surface cracks. *Sens. Actuat. A Phys.* **2011**, *170*, 55–61. [[CrossRef](#)]
22. Tehranchi, M.M.; Hamidi, S.M.; Eftekhari, H.; Karbaschi, M.; Ranjbaran, M. The inspection of magnetic flux leakage from metal surface cracks by magneto-optical sensors. *Sens. Actuat. A Phys.* **2011**, *172*, 365–368. [[CrossRef](#)]
23. Wu, B.; Wang, Y.J.; Liu, X.C.; He, C.F. A novel TMR-based MFL sensor for steel wire rope inspection using the orthogonal test method. *Smart Mater. Struct.* **2015**, *24*, 075007. [[CrossRef](#)]
24. Julliere, M. Tunneling between ferromagnetic films. *Phys. Lett. A* **1975**, *54*, 225–226. [[CrossRef](#)]
25. Ye, S.K. Test and Development of the Wireless ACFM Detection Instruments. Master's Thesis, Nanchang Hangkong University, Nanchang, China, 2016.
26. Wang, P.; Gao, Y.; Tian, G.; Wang, H. Velocity effect analysis of dynamic magnetization in high speed magnetic flux leakage inspection. *NDT E Int.* **2014**, *64*, 7–12. [[CrossRef](#)]
27. Lyu, Z.; Karcher, C. Non-contact electromagnetic flow measurement in liquid metal two-phase flow using Lorentz force velocimetry. *Magneto hydrodynamics* **2017**, *53*, 67–77. [[CrossRef](#)]

**Disclaimer/Publisher's Note:** The statements, opinions and data contained in all publications are solely those of the individual author(s) and contributor(s) and not of MDPI and/or the editor(s). MDPI and/or the editor(s) disclaim responsibility for any injury to people or property resulting from any ideas, methods, instructions or products referred to in the content.